ARMY RESEARCH LABORATORY

Simulation of Organic Magnetic Resonance Force Microscopy Experiments

by Doran D. Smith

ARL-TR-4016 **December 2006**

NOTICES

Disclaimers

The findings in this report are not to be construed as an official Department of the Army position unless so designated by other authorized documents.

Citation of manufacturer's or trade names does not constitute an official endorsement or approval of the use thereof.

Destroy this report when it is no longer needed. Do not return it to the originator.

Army Research Laboratory
Adelphi, MD 20783-1197

ARL-TR-4016 **December 2006**

Simulation of Organic Magnetic Resonance Force Microscopy Experiments

Doran D. Smith
Sensors and Electron Devices Directorate, ARL

REPORT DOCUMENTATION PAGE

Form Approved
OMB No. 0704-0188

1. REPORT DATE *(DD-MM-YYYY)*	2. REPORT TYPE	3. DATES COVERED (From - To)
December 2006	Final	FY 2006

4. TITLE AND SUBTITLE
Simulation of Organic Magnetic Resonance Force Microscopy Experiments

5a. CONTRACT NUMBER

5b. GRANT NUMBER

5c. PROGRAM ELEMENT NUMBER

6. AUTHOR(S)
Doran D. Smith

5d. PROJECT NUMBER

5e. TASK NUMBER

5f. WORK UNIT NUMBER

7. PERFORMING ORGANIZATION NAME(S) AND ADDRESS(ES)
U.S. Army Research Laboratory
ATTN: AMSRD-ARL-SE-EO
2800 Powder Mill Road
Adelphi, MD 20783-1197

8. PERFORMING ORGANIZATION REPORT NUMBER
ARL-TR-4016

9. SPONSORING/MONITORING AGENCY NAME(S) AND ADDRESS(ES)
U.S. Army Research Laboratory
2800 Powder Mill Road
Adelphi, MD 20783-1197

10. SPONSOR/MONITOR'S ACRONYM(S)

11. SPONSOR/MONITOR'S REPORT NUMBER(S)

12. DISTRIBUTION/AVAILABILITY STATEMENT
Approved for public release; distribution unlimited.

13. SUPPLEMENTARY NOTES

14. ABSTRACT
This report describes the numerical simulation of a series of proposed magnetic resonance force microscopy (MRFM) experiments on organic material. The simulation predicts the performance of a new MRFM system under construction at ARL for use on 2-D and 3-D proton containing samples. The SNR's and signal lineshapes of the new MRFM system are predicted using a geometry and experimental protocol well suited to the study of organic materials.
The SNR for a 2-D proton monolayer with a density of one proton per square nanometer with one second of integration time over an optimized area will be one. For a 3-D sample the SNR is position dependent, but for a sample with one proton per cubic nanometer and one second integration time, the SNR always significantly exceeds one.
The strong SNR's in both the 2-D and 3-D cases makes observing a signal easy, and warrants continuing with the new organic MRFM system.

15. SUBJECT TERMS
Nuclear magnetic resonance, force detection, organic, MRFM

16. SECURITY CLASSIFICATION OF:			17. LIMITATION OF ABSTRACT	18. NUMBER OF PAGES	19a. NAME OF RESPONSIBLE PERSON
a. REPORT	b. ABSTRACT	c. THIS PAGE			Doran D. Smith
Unclassified	Unclassified	Unclassified	U	30	19b. TELEPHONE NUMBER (*Include area code*) (301) 394-1918

Standard Form 298 (Rev. 8/98)
Prescribed by ANSI Std. Z39.18

Contents

List of Figures

List of Tables

1. Introduction

This report describes a series of numerical simulations predicting the performance of a magnetic resonance force microscopy (MRFM) (*1*) system undergoing construction at Army Research Laboratory (ARL). The purpose of the simulations was to determine if the system performance is sufficient to warrant program continuation. The sample characteristics assumed in the simulation correspond to two-dimensional (2-D) and three-dimensional (3-D) proton-containing organic materials of direct relevance to ARL's mission program. The MRFM system characteristics assumed include a probe head and geometry optimized for the study of organic materials. This report describes the methods and experimental protocols that will be used by the new MRFM system. It then gives a detailed listing of the relevant parameters of the MRFM system, followed by a description of the mathematical model of the system. The results of the simulation are tabulated and discussed. The conclusions describe the substantiated findings of the simulation, describe their implications for future work, and include the author's opinion about the direction the program should take.

2. Methods

The most critical element of an MRFM system is the region where the MRFM signal is generated, the probe head. In order that large samples can be used while satisfying all the nuclear magnetic resonance (NMR) selection rules, the geometry, springiness preservation by aligning magnetization (SPAM) was selected (*2*). Figure 1 illustrates the elements of the SPAM geometry.

The experimental protocol that we will use is cantilever-enabled readout of magnetization inversion transients (CERMIT) (*3*). The MRFM signal using the CERMIT protocol manifests itself as a change in the natural oscillation frequency (f_c) of a driven cantilever. The change in f_c is attributable to an effective change in the cantilever spring constant caused by inversion of the polarization in a sensitive slice with the appropriate RF sequence. Figure 2 shows the sensitive slice for a 3-D sample. To determine the size and characteristics of the signal, we wrote a package of Mathmatica[1] programs to simulate different aspects of the experiment. The simulation is fully 2-D and 3-D as appropriate and accounts for the actual shape of the sensitive slice generally by a magnetic dipole. The simulation covers two different cases: 1) signal from a 2-D thin film, and 2) signal from a 3-D volume. For this situation, a 2-D thin film means all the spins in the thin film are

[1]Mathmatica is a registered trademark of Wolfram Research.

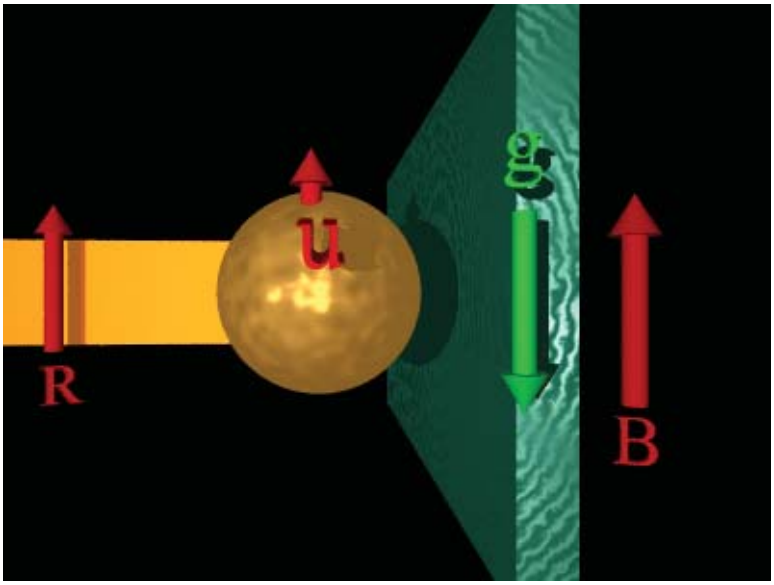

Figure 1. Magnetic particle with magnetic moment μ mounted on a cantilever that rotates about axis R. (The particle's magnetic moment μ is parallel to the back ground magnetic field B. When the cantilever oscillates, the magnetic particle's magnetic moment remains parallel to the background magnetic field, and thus it experiences no torque. Gravity g is down, although other orientations are possible. The sample is shown in green.)

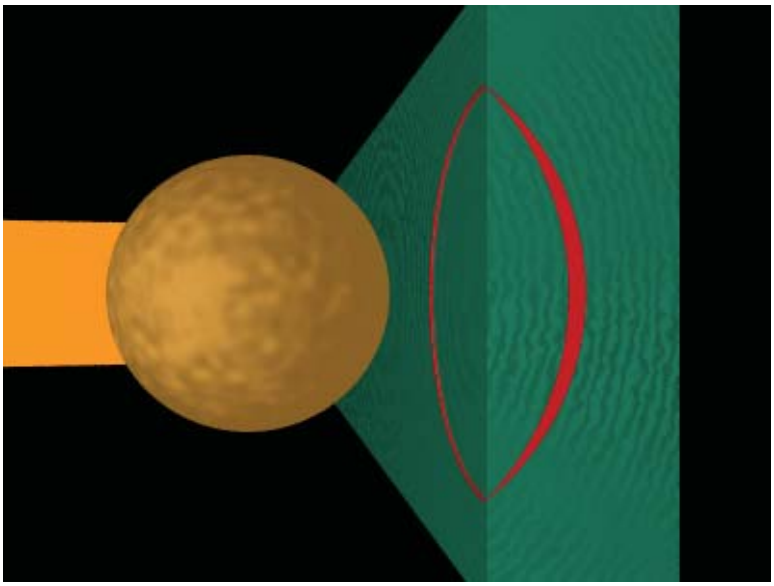

Figure 2. An artist's sketch of the 3-D sensitive slice shown in red.

contained within the thickness of the sensitive slice. Thus, the 2-D system can actually have a several-nanometer thickness.

The sensitive slice for a 2-D sample is a sensitive area as shown in figure 3. The oval shaped area of spins can be inverted with the appropriate RF sequence. To give the largest MRFM signal with a single spin inversion an oval centered under the magnet is inverted. The oval has a major and minor axis of 0.6 and 0.3, respectively, of the magnet diameter and is defined as the resolution when one is discussing 2-D images.

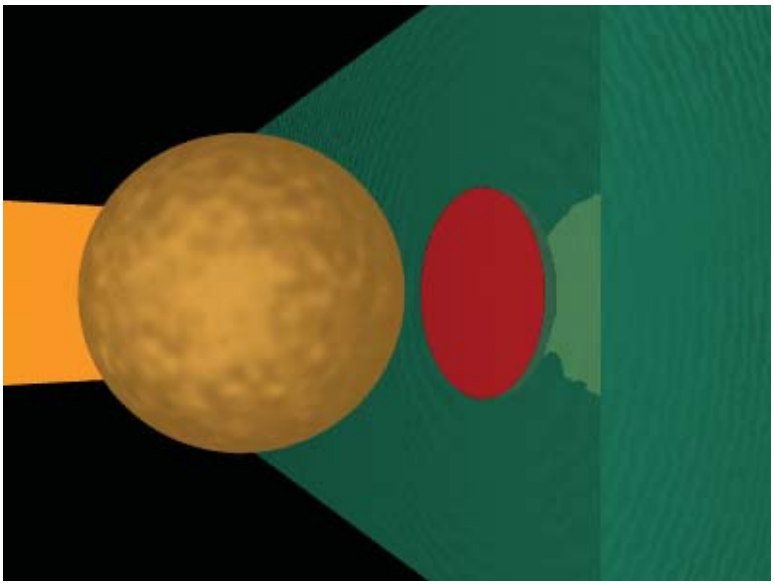

Figure 3. An artist's sketch of the 2-D sensitive area shown in red. The sensitive area is an oval centered under the magnet.

When one is discussing 3-D samples, the sample volume directly under the magnetic particle is the region from whence the imaging slices come. In this region, good spatial resolution is obtained with narrow sensitive slices. The sample outside this region contributes to the bulk peak (*4*). Figure 4 illustrates the two different regions.

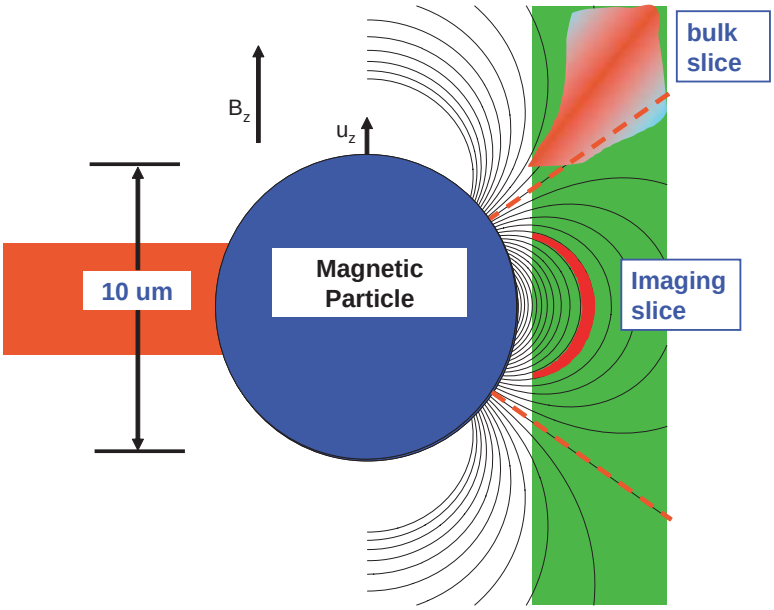

Figure 4. The background magnetic field is B_z and parallel to it is the magnetic particle's magnetic moment μ_z. (The contour lines represent iso-B_z surfaces. Above the top red dashed line and below the bottom red dashed line B_z is positive (parallel to the drawn vector B_z). In between the two red dashed lines B_z is negative. The two dashed red lines are drawn at the "magnetic angle," the angle at which, for a magnetic dipole, B_z is zero. The imaging slices occur directly beside the magnet and are typically less than one magnet radius from the magnet surface. The bulk slices occur predominantly outside the magnet diameter and can be a distance anywhere from several to an infinite number of times the magnet diameter away from the magnet.)

3. System Description

The simulation assumed an MRFM system with a spherical magnetic particle 10 μm in diameter mounted on a cantilever with a 100 μN/m spring constant, a mechanical Q of 10,000, and a resonance frequency of 1000 Hz. The spacing between the surface of the magnetic particle and the sample surface is 0.5 μm. The temperature of the cantilever and sample is assumed to be 5 K and the magnetic field 9 T.

All values in this report are derived with the parameters given in table 1.

Table 1. System parameters used in this report.

symbol	**value**	**units**	**description**
f_c	1000	Hz	cantilever resonance frequency
Δf_c	-	Hz	change in cantilever resonance frequency
$\Delta f_{\mathrm{C}}^{\mathrm{thermal}}$	25.9 $\times 10^{-6}$	Hz	Frequency noise attributable to Brownian motion of cantilever
Q	10000	-	cantilever mechanical quality factor
k	100	uN/m	cantilever spring constant
T	5.0	K	sample and cantilever temperature
b	1	Hz	bandwidth of sampling time
X_{rms}	2.857×10^{-6}	m	RMS value of cantilever drive. Peak-to-peak is 80% of magnet diameter
a	5	um	magnet radius
M	0.85	T	Magnet magnetization for SmCo
F_x	-	N	Force on cantilever in x direction
F_{min}	2.1 $\times 10^{-17}$	N	minimum detectable force attributable to Brownian motion of the cantilever
δx	0.5	um	separation between magnetic surface and sample surface
$\mu(r_i)$	-	J/T	magnetic moment of spin at location r_i
$\mu(\rho_{3D})$	10^{27}	m^{-3}	3D spin density of 1 proton/nm^3
$\mu(\rho_{2D})$	10^{18}	m^{-2}	2D spin density of 1 proton/nm^2
p	0.0019	-	Boltzmann polarization for protons at 5 K and 9 T
B_z, B_x, B_r	-	T	z, x, and radial components of the magnetic field
δB_z	10	mT	sensitive slice thickness
$\frac{\partial B_z}{\partial x}$	-	T/m	gradient of B_z in the x direction
$\frac{\partial^2 B_z}{\partial x^2}$	-	$\mathrm{T/m}^2$	second gradient of B_z in the x direction

4. Procedures - Description of the Mathmatical Model

The CERMIT protocol (*3*) relies on the interaction of the sample spins with magnetic field gradients from the magnetic particle to produce a net force gradient given by (this report and the simulation package are written in SI units)

$$\frac{\partial F_x}{\partial x} = -\sum_i \mu(r_i) \frac{\partial^2 B_z(r_i)}{\partial x^2} \tag{1}$$

in which B_z is the z component of the magnetic field attributable to the magnetic particle, r_i is the location of each spin $\mu(r_i)$, x is the direction of the cantilever deflection, and the sum is over all spins inverted by the RF. More recent derivations of equation 1 by the Marohn group at Cornell University multiply the right-hand side by an additional factor of two. If the more recent calculation is correct, all the signal to noise ratios (SNR's) listed in this report can be doubled. In both the 2-D and 3-D cases, we do not sum over a finite spin system but integrate over a spin density. In 3-D the intergral is

$$\frac{\partial F_x}{\partial x} = -\int_V \mu(\rho) \frac{\partial^2 B_z(\rho)}{\partial x^2} dV \tag{2}$$

in which $\mu(\rho)$ is a volume spin density. In 2-D $\mu(\rho)$ is an area spin density and the integration is over an area.

The force gradient changes the cantilever's effective spring constant which changes its resonant frequency by an amount

$$\Delta f_c \approx \frac{f_c}{2k} \frac{\partial F_x}{\partial x} \tag{3}$$

in which k is the cantilever spring constant and f_c is the resonant frequency of the cantilever.

The simulation integrates equation 2 over the sensitive slice. The limits of the integration are determined by two iso-B_z surfaces and the sample surfaces. The iso-B_z surfaces and width of the sensitive slice are determined by the magnetic field value, its gradient, and the applied RF.

The equations for the z and r (radial) components of the magnetic field from a magnetic dipole (*5*) located at the origin (x=0, y=0, z=0) at the arbitrary Cartesian point (x,y,z) is

$$B_z = \frac{a^3\,M}{3}\left(\frac{3\,z^2}{(x^2+y^2+z^2)^{\frac{5}{2}}} - \frac{1}{(x^2+y^2+z^2)^{\frac{3}{2}}}\right) \tag{4}$$

$$B_r = a^3\,M\,\frac{z\,\sqrt{x^2+y^2}}{(x^2+y^2+z^2)^{\frac{5}{2}}} \tag{5}$$

The gradients of B_z with respect to x are

$$\frac{\partial B_z}{\partial x} = a^3\,M\left(\frac{-5\,x\,z^2}{(x^2+y^2+z^2)^{\frac{7}{2}}} + \frac{x}{(x^2+y^2+z^2)^{\frac{5}{2}}}\right) \tag{6}$$

$$\begin{aligned}\frac{\partial^2 B_z}{\partial x^2} &= a^3\,M\,(\frac{35\,x^2\,z^2}{(x^2+y^2+z^2)^{\frac{9}{2}}} \\ &\quad -\frac{5\,(x^2+z^2)}{(x^2+y^2+z^2)^{\frac{7}{2}}} \\ &\quad +\frac{1}{(x^2+y^2+z^2)^{\frac{5}{2}}})\end{aligned} \tag{7}$$

5. Algorithm Used to Calculate Δk

To determine Δf_c given by equation 3, the intergral in equation 2 must be performed. The integral over all sensitive slices is determined with an efficient algorithm using just one pass through the sample volume. The algorithm is attributable to Dr. Kent Thurber (*5*), a former ARL post docorate now at National Institute of Health. The efficiency of the algorithm was further improved by Dr. Smith who removed the innermost loop and replaced it with a float to integer conversion.

The simulation is a five-step process. The user determines 1) the minimum and maximum values of B_z; the user does this from prior knowledge of the geometry. 2) The user decides on the size of dV, the Cartesian integration volume. Several different dV's can be used, depending upon the region of space being summed over. Varying the size of dV is useful as the dV to magnetic particle distances become larger. The farther from the magnetic particle dV is, the slower the magnetic field changes and the larger dV can become. This results in an integration over a user-controlled variable size grid and is useful for determining the behavior of the bulk peak. 3) An array full of zeros is created with the number of array elements equal to the desired number of sensitive slices. A mapping is defined between the range of expected B_z's and each array index. For example, a B_z range

of 0.0 to 0.2 T could be broken into 200 sensitive slices corresponding to 10 mT each. 4) The z-component of the magnetic field B_z from the magnet is evaluated at the center of each volume element. If B_z falls between 0 and 10 mT, the product $\frac{\partial^2 B_z}{\partial x^2} \times dV$ is summed into array element 1. If B_z falls between 10 and 20 mT, $\frac{\partial^2 B_z}{\partial x^2} \times dV$ is summed into array element 2. If B_z falls between 290 and 300 mT, $\frac{\partial^2 B_z}{\partial x^2} \times dV$ is summed into array element 29. Thus, a histogram of the intergral of $\frac{\partial^2 B_z}{\partial x^2} \times dV$ for all values of magnetic field is built in the array. This is done in just one pass through all the volume elements and just one evaluation of B_z and $\frac{\partial^2 B_z}{\partial x^2} \times dV$ for each dV. 5) The array of force gradients corresponding to each sensitive slice is then converted to frequency shifts via equation 3.

An identical procedure is used for 2-D except sums over areas are performed instead of sums over volumes.

6. Results

6.1 Magnetic Field Contours

The simulation used a Cartesian coordinate system with 10 μm diameter magnetic particle centered at $x = y = z = 0$. The long axis of the cantilever is parallel to the y-axis and the cantilever oscillates in the x direction. The sample surface lies and the xz plane at $y = 5.5$ μm. The distance from the magnetic particle surface to the sample surface is 0.5 μm. Figure 4 is a contour plot in the xz plane of iso-B_z surfaces spaced by 10 mT for a magnetic dipole. Figure 5 is a contour plot of the iso-B_z surfaces in the plane of the sample surface which lies in the xz plane 0.5 μm from the surface of the magnetic particle.

Figure 6 is a contour plot in the plane of the sample surface of the iso-$\frac{\partial B_z}{\partial x}$ surfaces for the magnetic field shown in figure 5. Figure 7 is a contour plot in the plane of the sample surface of the iso-$\frac{\partial^2 B_z}{\partial x^2}$ surfaces for the magnetic field shown in figure 5. Figure 7 is a map of the force gradient on which the SPAM protocol is based.

6.2 Convergence versus Size of Volume Element

Studies of signal strength versus dV and distance between the magnetic particle surface to sample surface were performed. The same dV is used throughout the entire imaging volume. Two criteria are used to determine a sufficiently small dV; dV is reduced until 1) equation 2 no longer changes and 2) the volume for each sensitive slice varies smoothly from one sensitive slice to the next sensitive slice. A cubic dV was used with all functions being evaluated at the center of the volume. The dV = $(25\text{ nm})^3$ is small enough that the

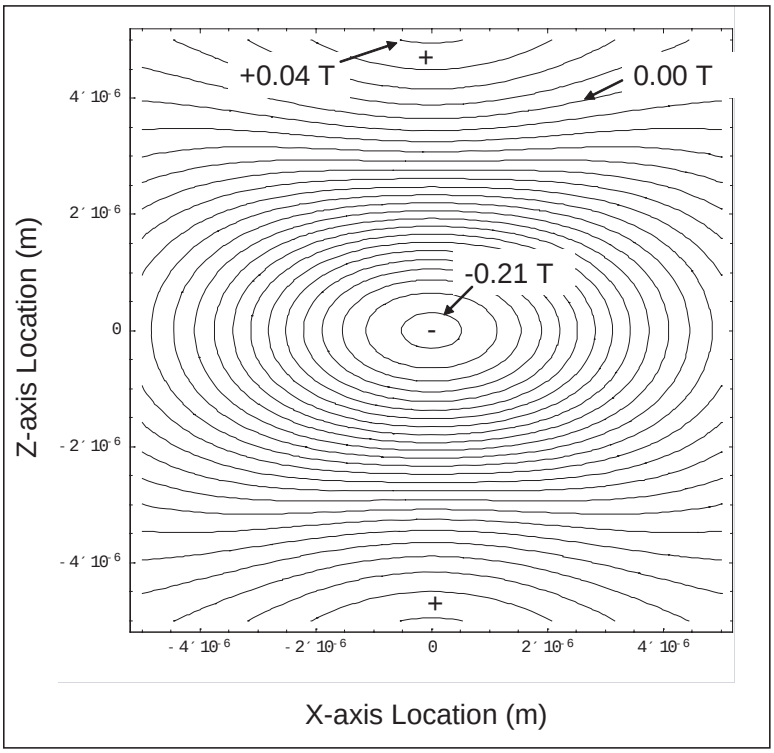

Figure 5. Iso-B_z for the geometry shown in figure 4 in the XZ plane at $y = 5.5\ \mu m$, the sample surface.

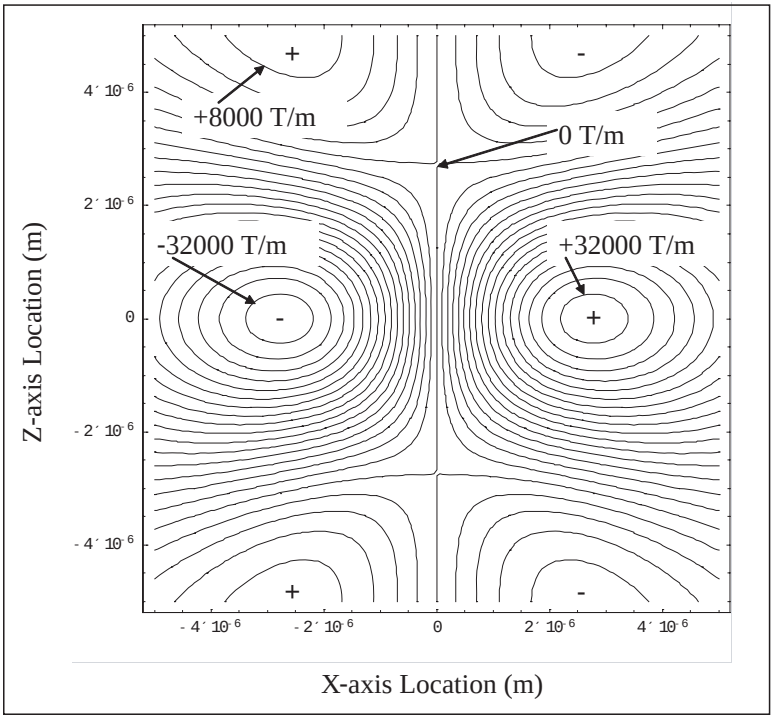

Figure 6. Iso-$\frac{\partial B_z}{\partial x}$ for the geometry shown in figure 4 in the XZ plane at $y = 5.5\ \mu$m, the sample surface.

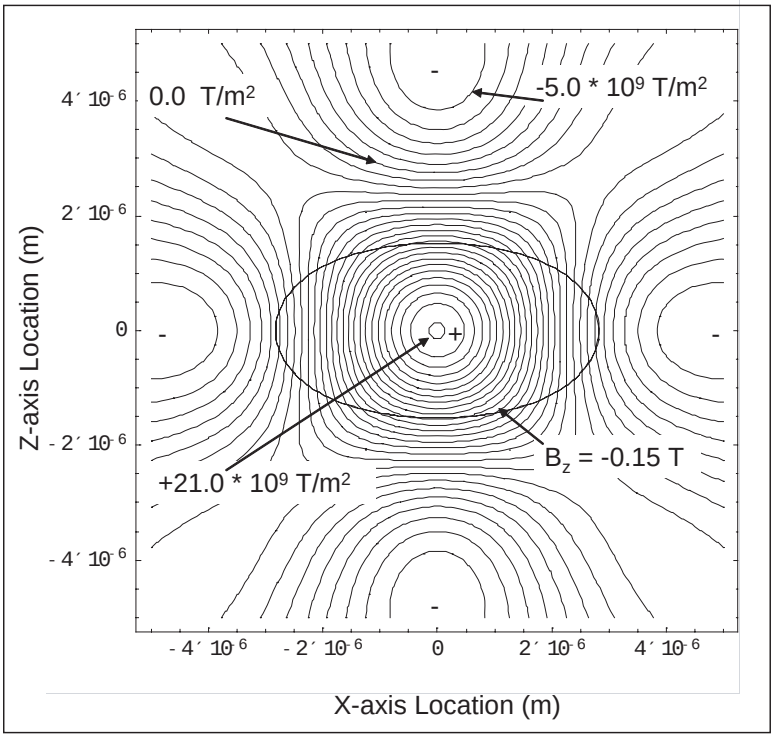

Figure 7. Iso-$\frac{\partial^2 B_z}{\partial x^2}$ for the geometry shown in figure 4 in the XZ plane at $y = 5.5$ μm sample surface. (The $\frac{\partial^2 B_z}{\partial x^2}$ yields the force gradient signal which manifests itself as a frequency shift of the driven cantilever. An iso-$B_z = -0.15$ T surface (oval in diagram center) is drawn corresponding to the optimal area or 80% of the first signal peak in figure 8.)

result is believed to be correct for 3-D. This approach calculated the volume to within 5 ppm of its true volume.

Larger volumes of varying sizes were used in the region containing the bulk peak. However, this work remains incomplete and is not discussed in this report. The issue to be addressed is convergence of integrals over an semi-infinite volume. Experimentally, the bulk peak is interesting and useful because it is narrow and large in intensity; however, the information that we typically wish to extract from the MRFM signal is all contained in the imaging slices. The bulk peak represents a result obtainable from conventional NMR and does not require MRFM.

The signal size Δf_c versus the magnetic particle surface to sample surface separation was studied. It was found of that for spacings greater than 1/20 the magnet diameter, the signal size decreased rapidly, but for separations less than 1/20 the magnet diameter, there are only marginal gains in signal size.

6.3 Comparison of Imaging Slices: 2-D versus 3-D and Smith versus Marohn

The results of the simulation were checked two ways. First, Smith checked his 3-D results obtained with a program he wrote in Mathmatica, against 3-D results that Dr. John Marohn of Cornell University obtained with a program he wrote in MATLAB[2]. Both simulations gave the same 3-D results.

To check the results of his 2-D simulation, Smith compared his 3-D simulation, using a 10 nm thick sample, to his 2-D simulation where he uses MATHMATICA's 2-D integration package to perform the integration. Both the 2-D and 3-D simulations gave the same results.

We therefore have a reasonable degree of confidence in the results of the simulation package. However, the checks were for a geometry known as the "hang down" geometry instead of the SPAM geometry described in this technical report. The only difference between the geometries, as far as the simulation is concerned, are angular factors.

6.4 Result: Optimal Integration Area in 2-D

For the integration of equation 2, we used the algorithm described previously. We performed the 2-D integral of $\frac{\partial^2 B_z}{\partial x^2}$ between two iso-B_z surfaces centered on the y-axis in the XZ plane of the 2-D sample. These iso-B_z surfaces are shown in figure 5. The origin represents the inner (larger B_z value) iso-B_z surface while one of the contour lines represents the outer (smaller B_z value) iso-B_z surface. With the appropriate RF protocols,

[2]MATHLAB is a registered trademark of MathWorks.

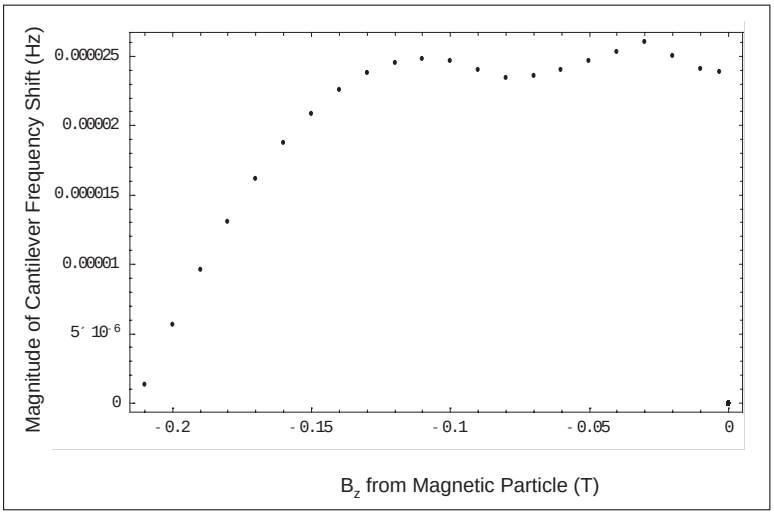

Figure 8. The frequency shift of the cantilever versus iso-B_z surface from the magnetic particle. (The proton spins are inverted for the area between two iso-B_z surfaces. The first surface $B_z \approx -0.21$ T occurs at $x = 0$ and $z = 0$. The second surface is given on the diagram's x-axis. The signal peaks for the first time at iso-$B_z = -0.11$ T. The contour shown in figure 7 is for the iso-B_z surface $B_z = -0.15$ mT. See text for discussion.)

the spins between any two iso-B_z surfaces can be inverted. By determining the signal size as a function of the outer surface, we can determine the optimal area over which to invert the spins to obtain the maximum signal. Figure 8 is an illustration of equation 2 versus the outer iso-B_z surface where the inner surface is always assumed to be the Y-axis where $B_z = -0.21$ T. We see that for a 10 μm diameter magnetic particle, the signal peaks for an area contained between $B_z = -0.21$ T and $B_z = -0.11$ T. However, for an area contained between $B_z = -0.21$ T and $B_z = -0.15$ T, we get 80% of the signal but only half the area. Therefore, we call this the optimal area when discussing resolution in 2-D. This area is outlined near the center of figure 7 as an oval corresponding to the iso-B_z surface $B_z = -0.15$ T. Inversion of all the proton spins in the optimal area requires a rapid passage sweep 2.55 MHz wide. We see that the area begins in all positive $\frac{\partial^2 B_z}{\partial x^2}$ area and extends a little into the negative area along the x-axis. The advantage of extending a little into the negative area is that the integral picks up more positive area along the z-axis resulting in an overall net gain.

6.5 Result: Sensitive Slice Size for 3-D

With the parameters in table 1, a plot of the change in the cantilever frequency Δf_c for a sensitive slice width of 10 mT is shown in figure 10. The sample volume used is a right cylinder 5 μm in length with a 5 μm radius. The cylinder axis is parallel to the Y-axis, which is parallel to the surface normal. A sample volume this small only contains the

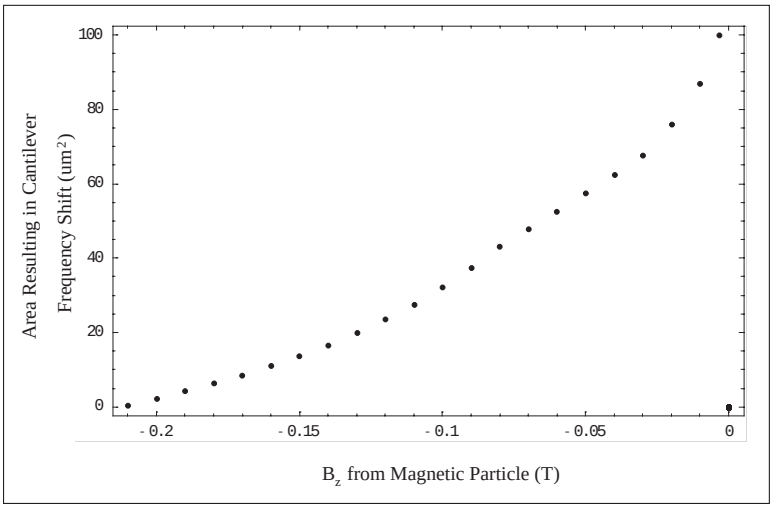

Figure 9. The area over which the proton spin density is inverted that results in the frequency shift shown in figure 8.

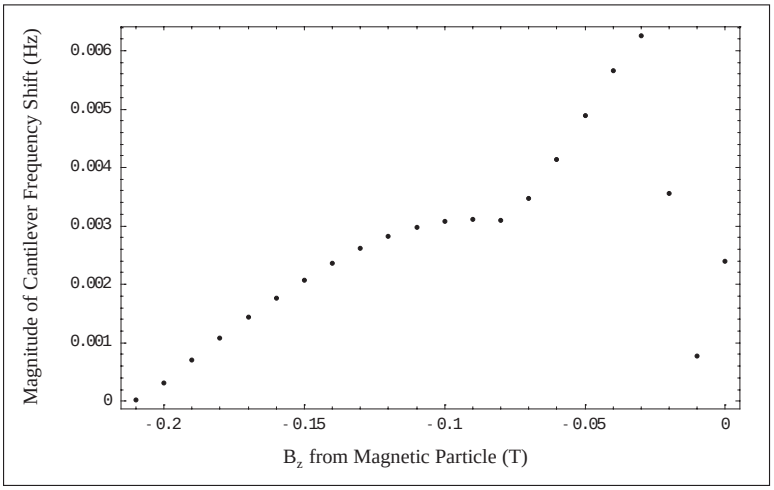

Figure 10. The frequency shift of the cantilever because of the inversion of the proton spins in a single sensitive slice versus the particle's magnetic field contribution to the total magnetic field at the sensitive slice. (The width of each sensitive slice is 10 mT. This iso-B_z spacing corresponds to the contour lines drawn in figure 4. See text for explanation of the behavior of the data near zero Tesla.)

imaging slices. The bulk slices are mainly outside this volume and are not protrayed correctly in figure 10. For magnetic field values as great as -0.03 T, the sensitive slices are contained entirely inside the sample volume. For magnetic field values larger than -0.03 T (-0.02 to 0.00 T - the rightmost four data points), the sensitive slices are leaving the sample volume and the frequency shift values are not correct.

The CERMIT signal shown in figure 10 has two competing effects: 1) the force gradient $\frac{\partial^2 B_z}{\partial x^2}$ is falling off very rapidly as the sensitive slice penetrates deeper into the sample.

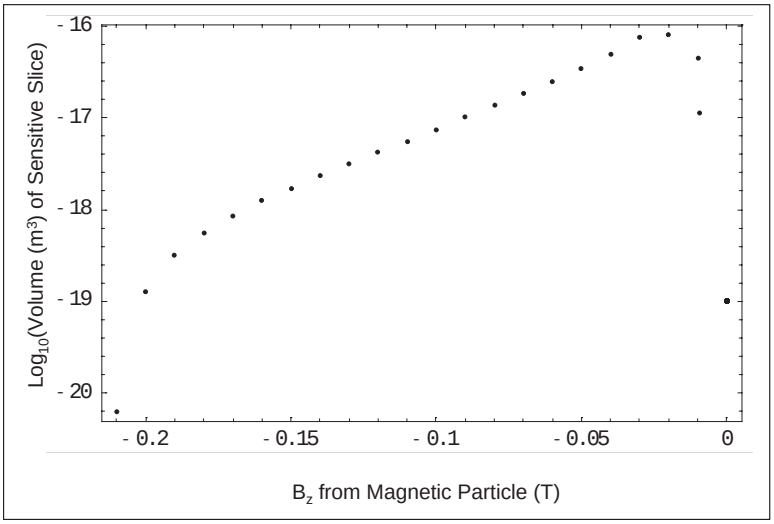

Figure 11. The Log_{10} of the volume of the sensitive slice versus the particle's magnetic field contribution at the sensitive slice. (See text for explanation of the behavior of the data near zero Tesla.)

However, this is counterbalanced by 2) a rapid growth in the sensitive slice of volume as shown in figure 11. For a depth change of only a magnetic particle radius, the sensitive slice volume increases by about three orders of magnitude. The increase in volume is more rapid than the decrease in force gradient and thus, the CERMIT signal grows with increasing depth into the sample as shown in figure 10.

Table 2 gives a summary of the results of the numerical simulation for varying magnet diameters. The volume spin density assumed is 1 proton/nm^3 and the area spin density assumed is 1 proton/nm^2. These results are easily scaled to the relevant spin density for a given sample. Table 2 does not list signal sizes but gives SNR. The noise floor for a well-designed MRFM experiment is the thermomechanical Brownian motion noise of the cantilever. For the CERMIT protocol, the Brownian motion manifests itself as changes in the cantilever resonant frequency and is approximately given by (*6*)

$$\Delta f_c^{thermal} \approx \frac{f_c}{2k} \times \frac{F_{min}}{\sqrt{2}X_{rms}} \tag{8}$$

where X_{rms} is in the rms amplitude of the driven cantilever and F_{min} is

$$F_{min} = \sqrt{4k_B T b}\sqrt{\frac{k}{Q 2\pi f_c}} \tag{9}$$

Table 2. Predicted SNR's (The parameters listed in table 1 were used to derive the results in this table. Areas, volumes, and SNR are listed as the magnet diameter is scaled down. The 2-D lateral resolution are the lengths of the major and minor axes of the oval shown in figure 7. The 2-D area is the actual area of the oval. The 3-D normal resolution is the sensitive slice thickness parallel to the normal of the sample surface. The 3-D lateral resolution is the length of the major and minor axes of the sensitive volume at the sample surface as shown in figure 13. The 3-D normal resolution is not given for the 200- and 50-nm-diameter magnets because the sensitive slice becomes so thin that other physics will dominate the resolution that the instrument is able to obtain. See text for description of the 3-D small and large sensitive slices.)

Magnet Diameter (nm)	**Magnet to Sample Separation (nm)**	**Slice**	**Resolution**		**2D Voxel Area (μm^2)**	**2D SNR $/\sqrt{Hz}$ (unitless)**	**3D Voxel Volume $(\mu)^3$**	**3D SNR $/\sqrt{Hz}$ (unitless)**
			Normal (nm)	**Lateral** (nm^2)				
10,000	500	2D area	-	3100 x 5700	13.76	1	-	-
		3D small	88	1200 x 3200	-	-	$(0.504)^3$	12.1
		3D large	700	6300 x 17700	-	-	$(3.66)^3$	218
2,000	100	2D area	-	620 x 1140	0.550	1	-	-
		3D small	18	240 x 640	-	-	$(0.101)^3$	2.4
		3D large	140	1260 x 3540	-	-	$(0.732)^3$	44
200	100	2D area	-	62 x 114	0.0055	1		-
		3D small	-	24 x 64	-	-	$(0.0101)^3$	2.4
		3D large	-	126 x 354	-	-	$(0.0732)^3$	44
50	2.5	2D area	-	13 x 23	0.000220	1	-	-
		3D small	-	4.8 x 12.8	-	-	$(0.00202)^3$	2.4
		3D large	-	25.2 x 71	-	-	$(0.0146)^3$	44

where k_B is Boltzman's constant, T the absolute temperature, b is the bandwidth of the measurement, and Q is the mechanical quality factor of the cantilever. The values of these quantities are given in table 1. Marohn *(7)* has determined that the optimal value for X_{rms} is approximately 0.8 of the magnetic particle diameter. The SNR given in table 2 is the ratio the signal size to the Brownian motion noise floor given by equation 8.

7. Discusion of Results

The SNRs are given for a 2-D density of 1 proton/nm^2. The typical organic sample will have a proton density many times (10 to 100) this number. However, the use of 1 p/nm^2 illustrates how sensitive the work will be to changes in the thin film's proton density. Given the large SNR, smaller resolutions are obtainable at the expense of decreased sensitivity. The actual limits to the lateral resolution in 2-D will be determined by the goal of the experiment, the details of the signal characteristics, and how long we are willing to integrate. The goals of each study will determine the trade-offs. There appears to be no reason why integration times cannot be hours.

The SNR for 3-D experiments is a function of the sensitive slice chosen. The deeper into the sample the sensitive slice is, the larger its volume becomes and the smaller the force gradient is. The volume becomes larger faster and thus the SNR increases as the sensitive slice sinks into the sample. However, after the depth becomes somewhat greater than a magnetic particle radius, the imaging slices began to evolve into the bulk peak and lose most their spatial resolution. The SNR is shown in table 2 is for two 3-D sample volumes at the limits of sensitive slice volumes, the smallest and the "largest" (see figure 12). The small volume is the first sensitive slice contained entirely within the sample volume and has a volume of 0.128 μm^3 = (0.50 μm)^3 for a 10 mT wide sensitive slice. A sensitive slice of 10 mT is very wide; slices as thin as 1 mT are possible. The "largest" sample volume chosen, is one of the largest volumes contained under the magnetic particle before the sensitive slice enters the bulk region. It has a volume of 49.0 μm^3 = (3.66 μm)^3.

7.1 Scaling Laws as the Magnetic Particle Size is Reduced Below 10 μm

For the 2-D work described here, as the magnetic particle size is scaled down, the SNR remains the same while the spatial resolution increases. The technical term for this is "a free lunch." In going from a 10 μm to 50 nm diameter magnetic particle, the 2-D spatial resolution improves (10000/50) = 200 times with no loss in signal. This can be understood if we realize that there are two competing effects that cancel each other. Let r be some characteristic dimension linear in the size of the magnet. For an area covered by spins, the numbers of spins decrease like the area or r^2, while the force gradient, equation 1, upon which the CERMIT protocol depends, contains two factors of length in its demonator and increases like r^2. Thus, the two effects cancel each other.

This scale independence is not preserved for 3-D. As the sensitive slice volume gets smaller by r^3, the force gradient only gets larger by r^2. Thus, the signal gets smaller by one factor of r as the magnet volume scales down like r^3. For 3-D while going from a 10 μm to 50 nm

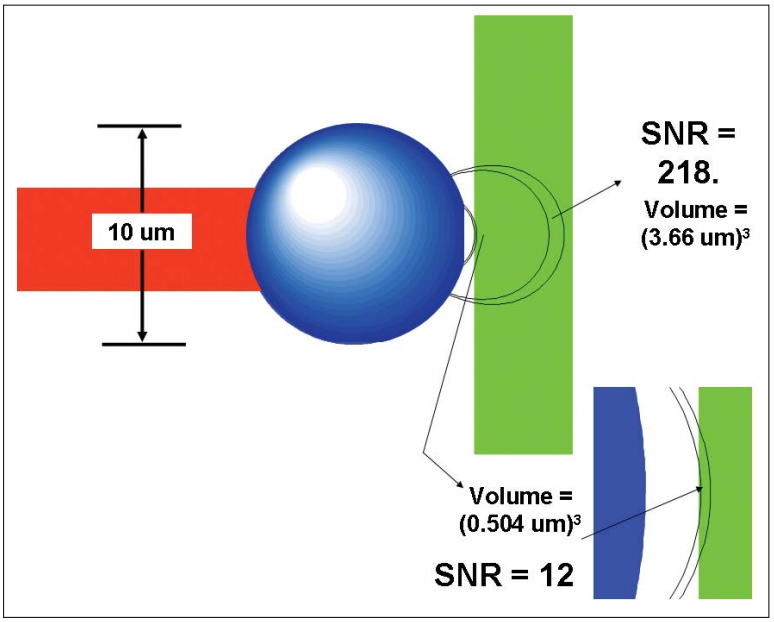

Figure 12. The SNR and volume of the smallest and largest sensitive slices 10 mT wide contained totally within a 5 μm thick sample. (In just four to five more sensitive slices beyond the large volume, they blow up into the bulk slice.)

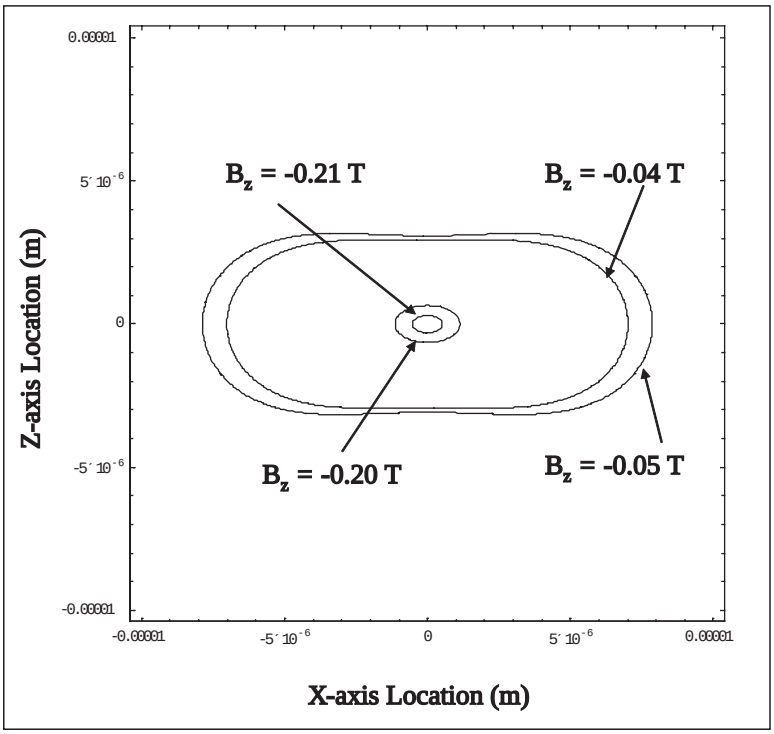

Figure 13. The iso-B_z surfaces shown define the limits of the 3-D large and small sensitive slices at the sample surface. (The penetration of these sensitive slices into the sample is shown in figure 12.)

diameter magnetic particle, the imaging volume improves like r^3 or $(10000/50)^3 = 8 \times 10^6$ times with a loss in signal size linear in r of 200.

The 10 μm diameter magnetic particle size used in this work is large for MRFM these days and only constitutes a starting point for the CERMIT work. This diameter sphere in the SPAM geometry using the CERMIT protocol will be used to determine the initial signal characteristics of our samples.

The 10 μm sphere will be glued onto the end of a cantilever with a micro-manipulator. An easy step beyond that is to Focus Ion Beam (FIB) the particle down in size. Rugar's team at IBM typically is able to FIB particles down to 200 nm. One can imagine intermediate steps at 1 to 2 μm and then 200 nm. Also, Marohn's group at Cornell University is developing 50 nm e-beam defined magnetic particles on cantilevers. Therefore, different paths exist that we can take on our way to greater resolution and sensitivity. What route to take will be determined as we learn more about the MRFM signal characteristics of our organic thin films.

8. Conclusions and Future Directions

The SNRs for 2-D and 3-D samples are large for the proton density simulated here. Actual proton densities are sample dependent of course but can easily be 10 to 100 times greater, and this would result in a corresponding SNR increase.

The author's recommendation is to continue with the construction of the organic MRFM system as the impact on current mission programs appears easy.

References

[1] Sidles, J. A. *Appl. Phys. Lett.* **1991**, *58*, 2854.

[2] Marohn, J. A.; Fainchtein, R.; Smith, D. D. *Appl. Phys. Lett.* **1998**, *73*, 3778.

[3] Garner, S. R.; Kuehn, S.; Dawlaty, J. M.; Jenkins, N. E.; Marohn, J. A. *Appl. Phys. Lett.* **2004**, *84*, 5091.

[4] Suter, A.; Pelekhov, D. V.; Roukes, M. L.; Hammel, P. *J. Meg. Res* **2002**, *154*, 210.

[5] Thurber, K. private communication.

[6] Marohn, J.; Muller, D. M.;Silveria, W. R. internal report.

[7] Marohn, J. private communication.

INTENTIONALLY LEFT BLANK

Distribution List

ADMNSTR
DEFNS TECHL INFO CTR
ATTN DTIC-OCP (ELECTRONIC COPY)
8725 JOHN J KINGMAN RD STE 0944
FT BELVOIR VA 22060-6218

DARPA
ATTN IXO S WELBY
3701 N FAIRFAX DR
ARLINGTON VA 22203-1714

OFC OF THE SECY OF DEFNS
ATTN ODDRE (R&AT)
THE PENTAGON
WASHINGTON DC 20301-3080

US ARMY TRADOC
BATTLE LAB INTEGRATION & TECHL DIRCTRT
ATTN ATCD-B
10 WHISTLER LANE
FT MONROE VA 23651-5850

SMC/GPA
2420 VELA WAY STE 1866
EL SEGUNDO CA 90245-4659

COMMANDING GENERAL
US ARMY AVN & MIS CMND
ATTN AMSAM-RD W C MCCORKLE
REDSTONE ARSENAL AL 35898-5000

US ARMY INFO SYS ENGRG CMND
ATTN AMSEL-IE-TD F JENIA
FT HUACHUCA AZ 85613-5300

US GOVERNMENT PRINT OFF
DEPOSITORY RECEIVING SECTION
ATTN MAIL STOP IDAD J TATE
732 NORTH CAPITOL ST., NW
WASHINGTON DC 20402

US ARMY RSRCH LAB
ATTN AMSRD-ARL-CI-OK-TP TECHL LIB
T LANDFRIED (2 COPIES)
BLDG 4600
ABERDEEN PROVING GROUND MD 21005-5066

DIRECTOR
US ARMY RSRCH LAB
ATTN AMSRD-ARL-RO-EV W D BACH
PO BOX 12211
RESEARCH TRIANGLE PARK NC 27709

US ARMY RSRCH LAB
ATTN AMSRD-ARL-CI-OK-T TECHL PUB (2 COPIES)
ATTN AMSRD-ARL-CI-OK-TL TECHL LIB (2 COPIES)
ATTN AMSRD-ARL-D J M MILLER
ATTN AMSRD-ARL-SE-EO D D SMITH
ATTN IMNE-ALC-IMS MAIL & RECORDS MGMT
ADELPHI MD 20783-1197

INTENTIONALLY LEFT BLANK